LAWRENCE
LIVERMORE
NATIONAL
LABORATORY

LLNL-PROC-645329

# Development, experimental performance and damage properties of x-ray optics for the LCLS free-electron laser

R. Soufli, E. T. Al

October 30, 2013

SPIE Damage to VUV, EUV, and X-ray Optics IV
Prague, Czech Republic
April 15, 2013 through April 19, 2013

## Disclaimer

# Development, experimental performance and damage properties of x-ray optics for the LCLS free-electron laser

Regina Soufli[1*], Mónica Fernández-Perea[1], Jacek Krzywinski[2], David W. Rich[2], Sherry L. Baker[1], Jeff C. Robinson[1], Stefan Hau-Riege[1], Eric M. Gullikson[3], Valeriy V. Yashchuk[3], Wayne R. McKinney[3], Philip Heimann[2], William F. Schlotter[2], Michael Rowen[2], Paul A. Montanez[2], Sébastien Boutet[2]

[1]Lawrence Livermore National Laboratory, 7000 East Avenue, Livermore, California, US

[2]SLAC National Accelerator Laboratory, 2575 Sand Hill Road, Menlo Park, CA 94025

[3]Lawrence Berkeley National Laboratory, 1 Cyclotron Road, Berkeley, CA 94720

## ABSTRACT

This manuscript presents an overview of recent work performed on x-ray optics development, metrology and calibration for the Soft X-ray Research (SXR) and the Coherent X-ray Imaging (CXI) instruments at the Linac Coherent Light Source (LCLS) free-electron laser. We also present results on the first LCLS exposures of boron carbide ($B_4C$)-coated samples at photon energies near the carbon K edge and discuss relevant analysis and implications for future experiments.

**Keywords:** free-electron lasers, x-ray optics, boron carbide, silicon carbide, damage, metrology, reflectivity.

## 1. INTRODUCTION

The development, fabrication and calibration of novel x-ray optics (mirrors and gratings) for the first set of instruments at the Linac Coherent Light Source (LCLS) facility has been completed. LCLS is the world's first x-ray free-electron laser (FEL) to have been operational, starting in 2009 and is located on the site of SLAC National Accelerator Laboratory[1]. In the soft x-ray regime, the LCLS photon energy range was initially planned to be 0.827 - 2 keV (in the 1st harmonic). Recently, the LCLS soft x-ray range has been extended to operate at photon energies as low as 0.2 – 0.3 keV. The first LCLS exposures at photon energies near 0.284 keV, the region of the carbon K absorption edge, are discussed later in this manuscript. The hard x-ray region of the LCLS includes all energies above 2 keV, with up to 11.2 keV having recently been demonstrated (1st harmonic). Higher photon energies are possible if the 3rd harmonic is used, with mirror reflectivity cutoff representing the ultimate limitation. The first x-ray optics in the path of the LCLS beam are the grazing incidence x-ray mirrors of the Front End Enclosure (FEE), the area located at the exit of the LCLS undulators. The FEE mirrors are used as low pass-filters that spectrally and physically separate the coherent FEL beam (before it enters the experimental areas) from high-energy spontaneous radiation, bremsstrahlung, γ-rays and their secondary products. In the soft x-ray branch, four FEE mirrors direct the FEL beam to the Soft X-ray Research (SXR) and the Atomic, Molecular and Optical science (AMO) experimental stations. In the hard x-ray branch, two FEE mirrors direct the FEL beam to the X-ray Pump-Probe (XPP), X-ray Correlation Spectroscopy (XCS), Coherent X-ray Imaging (CXI) and Materials under Extreme Conditions (MEC) experimental stations. Furthermore, two focusing mirrors are used at the AMO beamline and three mirrors and two gratings are used at the SXR beamline. The CXI beamline also uses two pairs of focusing mirrors and the MEC beamline uses one flat steering mirror. In collaboration with other national laboratories and commercial vendors, Lawrence Livermore National Laboratory (LLNL) led the design, specification, mounting, precision surface metrology and modeling of several of the x-ray mirrors installed at LCLS, including all the x-ray mirrors in the FEE[2,3,4,5].

Among the most distinctive properties of the LCLS beam are its extremely high brightness and coherence. The LCLS emits typically < 50 femtosecond x-ray pulses with ~0.3% bandwidth and with brightness equal to $10^{32}$ photons $sec^{-1}$ $mm^{-2}$ $mrad^{-2}$ (0.1% bandwidth)$^{-1}$. $B_4C$ and SiC were chosen as the reflective coating materials for the LCLS soft x-ray and hard x-ray optics respectively, due to their predicted high damage thresholds against the LCLS FEL beam compared

to other coating materials[6,7,8,9,10], combined with the good reflective performance and absence of electronic absorption edges in the originally planned energy ranges of operation of 0.827-2 keV (for $B_4C$ in the soft x-ray) and 2 -24 keV (for SiC in the hard x-ray). The $B_4C$ and SiC coatings of all LCLS x-ray mirrors[3,11,12,13,14] were developed at LLNL and were deposited by DC-magnetron sputtering[15] on precisely figured and polished Si substrates supplied by commercial vendors. The requirement for the x-ray optics to preserve the coherent wavefront of the LCLS FEL beam imposes extremely tight specifications for both the substrate figure and the coating uniformity and will be discussed later in this paper.

Section 2 in this manuscript presents an overview of the development and experimental performance of the most recently completed x-ray optics for two LCLS beamlines: the SXR and CXI instruments. Section 3 discusses the experimental results and analysis of the first exposures of $B_4C$ mirror coatings to the LCLS FEL beam at photon energies near the carbon K edge. Section 4 provides a summary and plans for future work.

## 2. DEVELOPMENT AND CALIBRATION OF X-RAY OPTICS FOR THE LCLS SXR AND CXI INSTRUMENTS

The SXR beamline[16] at the LCLS operates in the 0.5 keV – 2 keV photon energy range and can accommodate experimental configurations such as x-ray emission, coherent imaging, resonant scattering, photoelectron spectroscopy and x-ray absorption spectroscopy. The scientific experiments that can be performed at the SXR beamline cover a variety of fields such as catalysis, magnetism, correlated materials, clusters and biological structure. The x-ray optics of the SXR beamline include a monochromator[17], consisting of a pre-focusing mirror M1 and two varied-line spacing gratings G1 and G2, with resolving power around 5000. Downstream from the monochromator, mirrors M2, M3 form a Kirkpatrick-Baez pair, which can focus the beam to a spot size ranging from about 1 $mm^2$ to 2 $\mu m^2$. All Si mirror and grating substrates were manufactured by Carl Zeiss Laser Optics (Oberkochen, Germany). The two grating rulings were performed by Shimadzu Corporation (Japan). The mid-and high-spatial frequency roughness (MSFR and HSFR) of the three Si mirror substrates were examined by atomic force microscopy (AFM) and optical profilometry at LLNL and were found to be in the 0.1-0.3 nm rms range, within the 0.4 nm rms specification. The slope error of the mirror substrates was also verified via surface slope measurements with a long trace profilometer at Lawrence Berkeley National Laboratory (LBNL)[18]. The slope error was found to be < 0.2 μrad rms, within the specification of 0.3 μrad rms. A 37.4 nm –thick $B_4C$ coating especially optimized for the LCLS FEL conditions[3,11,12] was deposited on all SXR mirrors and gratings at LLNL. Coating thickness uniformity of 0.14 nm rms across clear apertures extending to 205 mm length was demonstrated for all $B_4C$ coatings. The demonstrated coating uniformity was well within the 1 nm rms specification, required to preserve the coherent wavefront of the LCLS source. To verify the integrity of the nanometer-scale grating structure, the grating substrate topography was examined by AFM, as-received by the vendor and after cleaning at LLNL. Fig. 1 shows an example of the measured topography from the 100 lines/mm grating substrate, before and after cleaning. Some high features (mostly apparent at the bottom of the grooves and likely associated with the grating fabrication process) are reduced after the cleaning process. The grating topography was also verified before and after $B_4C$ coating on a 100 lines/mm test grating. The reflective performance of the mirrors and the diffraction efficiency of the gratings were calibrated at beamline 6.3.2. of the Advanced Light Source (ALS) synchrotron at LBNL. More details about the development, metrology and calibration of the LCLS SXR optics can be found in Ref. 14.

The CXI instrument[19] is designed to make use of the unique brilliance of the x-ray pulses from the LCLS FEL to image single sub-micron particles. The near complete transverse coherence of the LCLS FEL allows single particles to be imaged at high resolution while the short pulse duration limits radiation damage during the measurement. In this manner, the CXI instrument allows imaging of biological samples beyond the damage limit that cannot be overcome with synchrotron sources. The CXI instrument includes two pairs of high-quality focusing mirrors (1 μm and 0.1 μm spot size) in a Kirckpatrick-Baez (KB) geometry. The two pairs of mirrors allow the experimenters to maximize the signal by better matching the beam size to the sample size. Each mirror consists of a Si substrate polished/figured into an elliptical shape, followed by a SiC coating with thickness in the 50-55 nm range. The four KB Si substrates were polished by JTEC Corporation (Japan) using the elastic emission machining (EEM) method[20]. The SiC coating was developed and deposited at LLNL[12]. The MSFR and HSFR of the Si substrates were verified at LLNL by AFM and optical profilometry measurements prior to SiC coating. Fig. 2 shows the power spectral density (PSD) curves from the vertically-focusing Si mirror substrate belonging to the 1 μm focusing KB pair. The PSD was computed[21] from the height data in each of the AFM and Zygo scans. The PSD was formed by first calculating a two-dimensional Fourier power spectrum of the height

data, and the spectrum was then averaged azimuthally around zero spatial frequency to produce a PSD with purely radial spatial frequency dependence. This approach works well for quasi-isotropic surfaces, such as the substrate surfaces discussed in this manuscript. The root-mean-square (rms) roughness $\sigma$ (MSFR or HSFR) is obtained by the expression

$$\sigma^2 = \int_{f_1}^{f_2} 2\pi f S(f) df \,, \qquad (1)$$

where $f$ is the spatial frequency, $S(f)$ is the surface PSD, and $f_1$, $f_2$ define the spatial frequency range of relevance. Typically, HSFR is computed by combining PSD curves from 10×10 μm$^2$ and 2×2 μm$^2$ AFM scans and MSFR is computed by combining PSD curves from 2× and 20× optical profilometer magnifications and 10×10 μm$^2$ AFM scans. The figure and slope errors of the Si substrates for the 1 μm focusing KB pair were also measured by high-resolution slope-measuring deflectometry by a third party[22] and were found to be in the range < 1 nm rms and 0.05 μrad rms respectively, across the 350 mm clear aperture length. These values are within the 1 nm rms and 0.25 μrad rms specifications for the figure and slope errors of the CXI mirrors. Details about the instruments employed to perform the metrology discussed in this Section can be found in the References provided herein.

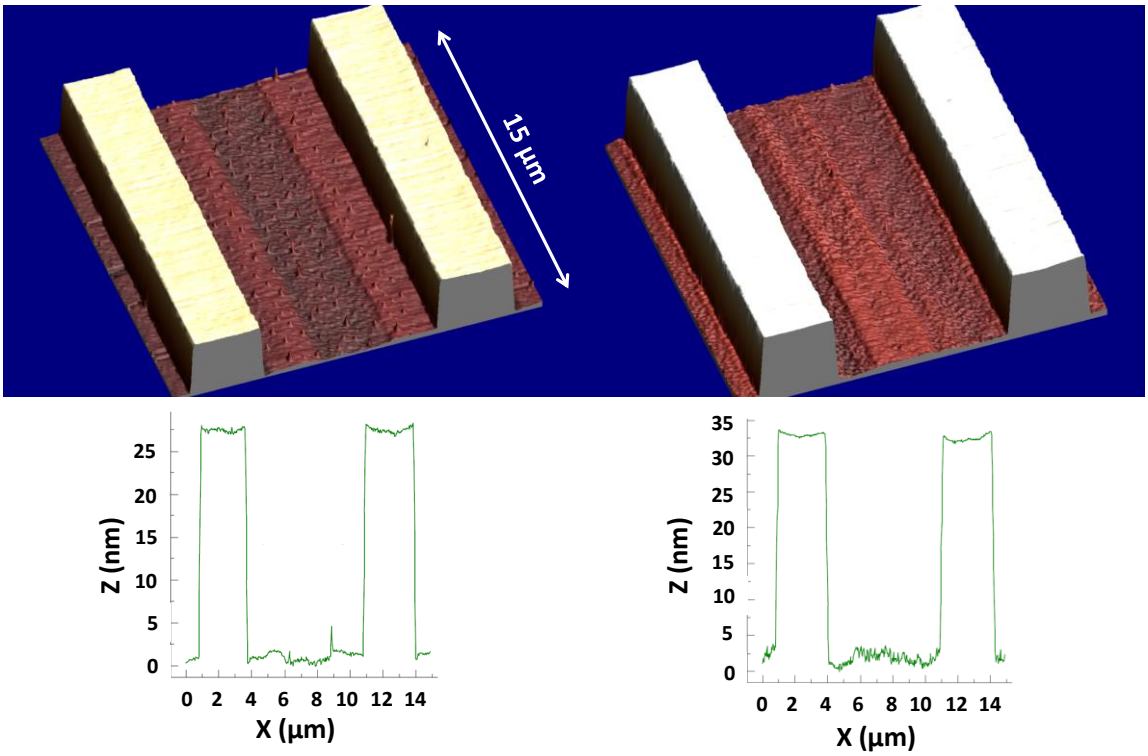


**Fig. 1:** 3-dimensional AFM images (top) and representative 1-dimensional line scans (bottom), obtained on the 100 lines/mm SXR Si grating substrate, prior to coating with $B_4C$. The software used to extract and analyze the 3-dimensional AFM images is described in Ref. 23. **Left:** 15×15 μm$^2$ scan, with the grating substrate as-received from the manufacturer. **Right:** 15×15 μm$^2$ scan, with the grating substrate after cleaning.

## 3. FIRST LCLS EXPOSURES AT PHOTON ENERGIES NEAR THE CARBON K-EDGE

During the Summer-Fall 2012 the operating photon energy range of the LCLS was extended and experiments were planned to include photon energies in the vicinity of the carbon K-edge (284.2 eV). Given the extremely high instantaneous dose of the LCLS FEL and the fact that the LCLS x-ray mirrors in the low-energy (soft x-ray) portion of the facility consist of $B_4C$ (i.e: carbon-containing) reflective coatings on silicon substrates, concerns arose about the safety and integrity of the $B_4C$-coated x-ray mirrors under irradiation by photon energies around the carbon K-edge. The concerns were motivated by accounts and published information[24] about enhanced carbon deposits and possibly other damage effects on mirrors irradiated by photon energies near the carbon K-edge, in various experimental facilities. To

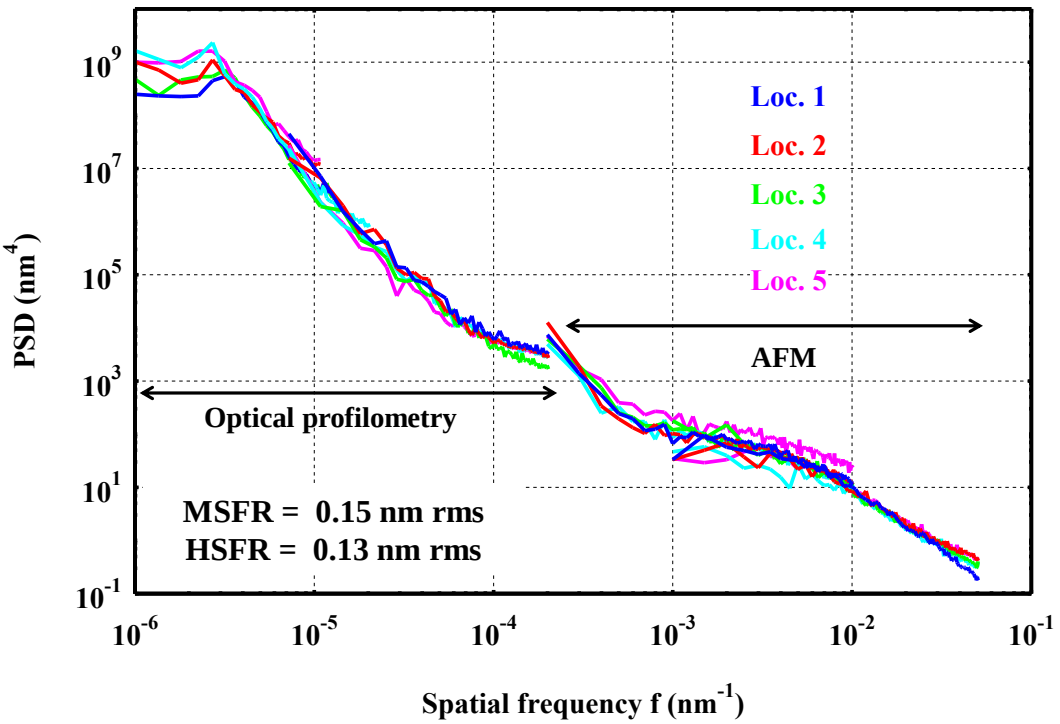


**Fig. 2:** Precision surface metrology results (optical profilometry and AFM) are shown, obtained on 5 locations across the 350 × 20 $mm^2$ clear aperture of one of the vertically-focusing Si mirror substrates of the CXI instrument. HSFR and MSFR values were computed from the plotted PSD curves according to Eq. (1) and were averaged between the 5 locations measured on the substrate. HSFR was computed in the spatial frequency range $f_1 = 5\times10^{-4}$ $nm^{-1}$, $f_2 = 5\times10^{-2}$ $nm^{-1}$ and MSFR was computed in the spatial frequency range $f_1 = 10^{-6}$ $nm^{-1}$, $f_2 = 5\times10^{-4}$ $nm^{-1}$.

address these concerns and to study any relevant phenomena, an experiment was planned to expose $B_4C$-coated samples at the LCLS at photon energies near the carbon K-edge. The samples consisted of a 55-nm thick $B_4C$ coating essentially identical to the reflective coatings of the LCLS soft x-ray mirrors[3,11,12] on a 525-µm-thick Si (100) substrate, deposited at LLNL and aged for about 3 years. The approximate dimensions of each sample were 20×20 $mm^2$. One sample (referred to as sample "f") was exposed at 295 eV (the photon energy reported in the literature[24] to incur the maximum carbon deposition upon irradiation) at 2 locations: one location was irradiated for 4 hours and a second, adjacent location was irradiated for 8 hours. A second, identical sample (referred to as sample "d") was exposed for 4 hours at 400 eV. The 400 eV photon energy was selected as a "control" energy, to compare with the results at 295 eV. The grazing incidence angle of the LCLS beam during the exposures was 0.8 degrees, same as the incidence angle on the $B_4C$-coated LCLS soft x-ray mirrors. The exposures took place in the X-ray Diagnostics Chamber (XDC). The XDC was located approximately 50 meters downstream from the end of the LCLS undulators. The FEL photon pulse energy was determined by measuring the electron beam energy loss due to the FEL action. The FEL process was switched off and on by kicking the electron beam orbit using a kicker magnet. Fig. 3 (left) shows an electron energy loss scan as a function of the magnetic field strength of the kicker magnet. Besides the $B_4C$-coated samples, the XDC also contained a Ce:YAG based x-ray beam profile monitor. A 0.5 µm thick CVD diamond foil was used to attenuate the X-ray beam in order to avoid Ce:YAG saturation. A typical profile of the LCLS photon beam inside the XDC chamber is shown in Fig. 3 (right), demonstrating an average full-width half-maximum (FWHM) beam size of 3.5 mm. The beam parameters and environment conditions during the LCLS exposures are summarized in Table 1.

After the LCLS exposures, the two samples underwent inspection with visible light under different illumination conditions, including high-intensity lamp in dark background. No visible differences were found between exposed and un-exposed areas on the samples. The exposed samples were also measured by AFM at LLNL. 2×2 and 10×10 $\mu m^2$ areas were scanned with the AFM at each measured location and a power spectral density (PSD) analysis was applied to determine the HSFR at each location. Sample "f" was measured at 3 locations: un-exposed (control), exposed at 295 eV

for 4 hours and exposed at 295 eV for 8 hours. The HSFR at these 3 locations was determined to be 0.61, 0.48 and 0.51 nm rms, respectively. Sample "d" was measured at 2 locations: un-exposed (control) and exposed at 400 eV for 4 hours. The HSFR at these 2 locations was determined to be 0.56 and 0.48 nm rms, respectively. The AFM images demonstrated uniform topography on all measured locations, with no significant differences in roughness between exposed and control (un-exposed) locations. During the AFM scans, it was observed that the exposed areas behaved in a different manner under the AFM tip than the control areas. This was a qualitative observation and did not translate into any significant differences in the AFM results. Sample "f" was also examined under an optical profilometer at LLNL, designated for measuring height variations in the spatial period range from a few tens of microns to about 1 mm. There were no significant height variations detected across the exposed vs. un-exposed areas of the sample. It is possible that any thickness changes between exposed and unexposed areas could be very gradual. This effect, combined with the very uniform topography of these samples, could make thickness changes difficult to capture with a profilometer instrument.

The exposed samples were measured at beamline 6.3.2.[25] of the ALS synchrotron at LBNL. Reflectance was measured vs. grazing incidence angle on different locations on each sample at 91.8 eV photon energy. The reflectance measurement geometry was such that the ALS photon beam was illuminating each sample along the same direction as the earlier LCLS beam exposures. The ALS beam size (~ 0.1 mm) was only a fraction of the LCLS beam size (~ 3.5 mm), with the latter determining the size of the LCLS-exposed areas. Therefore, this reflectance measurement allowed

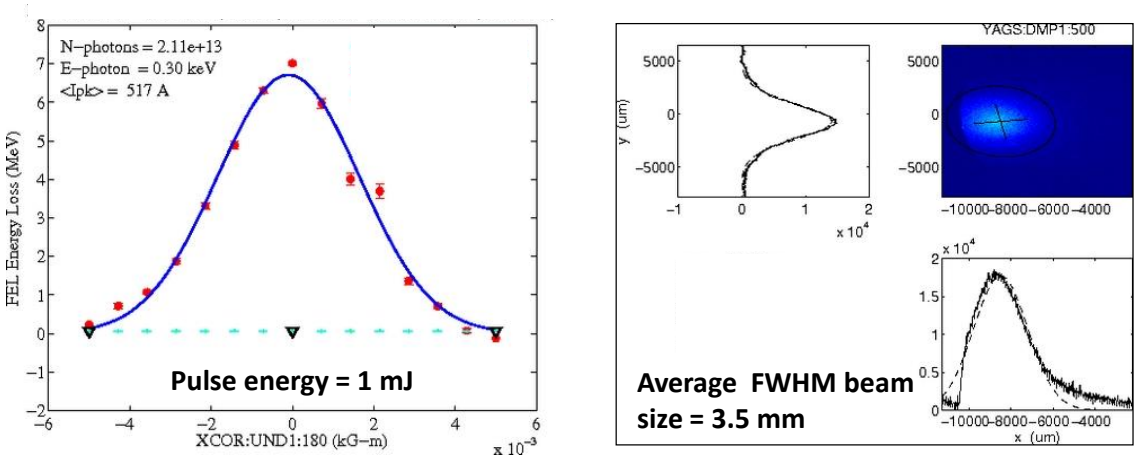


**Fig. 3: Left:** LCLS electron beam energy loss scan as a function of the magnetic field strength of the kicker magnet used to switch the FEL process on and off. This process was used to measure the LCLS FEL photon pulse energy at 295 eV. **Right:** Typical profile of LCLS photon beam inside XDC chamber.

## Irradiation conditions

| | |
|---|---|
| *Pulse energy* | 1 mJ |
| *Photon energies* | 295 eV and 400 eV |
| *Beam size* | 3.5 mm FWHM |
| *Repetition rate* | 120 Hz |
| *Incidence angle* | 0.8 deg |
| *Total pressure* | $10^{-8}$ Torr |
| *Hydrocarbon pressure (amu > 44)* | $10^{-11}$ Torr |
| *Exposure durations* | 4 and 8 hours at 295 eV<br>4 hours at 400 eV |

**Table 1:** Irradiation conditions of $B_4C$-coated samples during LCLS exposures.

the detailed scanning (with the ALS beam) of locations within and outside the LCLS-exposed areas on each sample. Fig. 4 shows the reflectance results from sample "f" obtained on 3 locations: un-exposed area, center of area exposed for 4 hours and center of area exposed for 8 hours at 295 eV at LCLS. The shift in Kiessig interference fringes among the 3 locations is indicative of a change in $B_4C$ coating thickness, if one assumes that the optical properties of the $B_4C$ coating remained the same before and after the exposures. Modeling[26] of the reflectance data using experimentally determined optical constants for the $B_4C$ coating[6] indicates erosion of the $B_4C$ coating thickness by 1 nm after 4 hours of LCLS exposure at 295 eV and by 1.6 nm after 8 hours of LCLS exposure at 295 eV. Fig. 5 shows the reflectance results from sample "d" obtained on 2 locations: un-exposed area and center of area exposed for 4 hours at 400 eV at LCLS. Modeling of the reflectance data from sample "d" indicates erosion of the $B_4C$ coating thickness by 1.3 nm after 4 hours of LCLS exposure at 400 eV. By comparing the results between the two samples, the amount (thickness) of the presumed erosion appears to be a function of the LCLS exposure time combined with the overall brightness of the LCLS beam at the photon energy of irradiation. No enhanced effects were observed on the sample exposed at 295 eV. If erosion were indeed the phenomenon responsible for the changes between exposed and un-exposed areas shown in Figs. 4 and 5, it may be worthwhile trying to understand its causes and mechanisms. It should be noted that, after long-term exposures in the LCLS mirror chambers, carbon-based deposits (not erosion) have been observed on the $B_4C$ coatings of the LCLS x-ray mirrors[13]. To explain this apparent contradiction, the following questions should be addressed: was the environment in the LCLS XDC chamber combined with the LCLS beam properties conducive to erosion? How would the LCLS XDC environment compare with the environments in the LCLS mirror chambers? Could a set of processes be present, where the observed erosion in the present short-term LCLS exposures is the pre-cursor to the formation of deposits that have been observed in the LCLS mirror chambers after longer-term exposures?

Another possible modification mechanism of the $B_4C$ coatings that could result in the shifts of the Kiessig fringes observed in Figs. 4 and 5 would be a change in the refractive index of the $B_4C$ coating material during the LCLS exposures. Fig. 6 shows modeling of the reflectance data from sample "f" at the center of the area exposed for 8 hours at 295 eV. The model that assumes a 1-layer "eroded" $B_4C$ coating, discussed in the previous paragraph, is compared with two other models: (i) a 2-layer "un-eroded" $B_4C$ coating, where the top 2 nm have a refractive index whose real (dispersive) part is 102% of the experimentally determined refractive index for $B_4C$[11] and (ii) a 2-layer "un-eroded" $B_4C$ coating, where the top 3.7 nm have a refractive index whose real part is 101% of the experimentally determined refractive index for $B_4C$. Among the 3 models, the 1-layer "eroded" model seems to fit best the Kiessig fringes occurring at angles away from grazing incidence, where the ALS beam used in the reflectance measurements probes deeper inside the coating. The other two models (2-layer "un-eroded" $B_4C$ coating with a change in the refractive index of the top layer) seem to fit better the grazing incidence region, around the critical angle. It should also be noted that, as has been shown earlier[11], the top ~9 nm of the $B_4C$ coating are oxygen- and carbon-rich. The above measurements, analysis and modeling indicate that both erosion and refractive index changes (or a combination of the two) may be plausible mechanisms to have occurred on the $B_4C$ coating during the LCLS exposures.

In order to further assess the effects discussed in the previous paragraphs, the penetration depth and dose values of the LCLS exposures described above were calculated vs. incidence angle. Figure 7 (a) shows calculated penetration depth values at 295 eV and 400 eV, for (i) the LCLS x-ray beam and (ii) a combination of the LCLS x-ray beam and secondary electrons generated during the interaction of the beam with the sample. The x-ray penetration depth was calculated using the formulae for evanescent waves on a semi-infinite solid from Ref. 27. The secondary electron penetration depth was estimated from an empirical formula in Ref. 28. The combined penetration depth is the sum of the two numbers. At 0.8 degrees (the incidence angle of the LCLS exposures) Fig. 7 (a) shows that the combined penetration depth is about 7 nm at 295 eV and 10 nm at 400 eV. The range of penetration depths is consistent with the results of the reflectance measurements and analysis discussed in the previous paragraphs. Fig. 7 (b) shows the dose (eV/atom) corresponding to the penetration depths plotted in Fig. 7 (a), where the dose is calculated as the incident intensity divided by the penetration depth. It is shown that at both 295 eV and 400 eV photon energies, the dose is well below the single-shot damage threshold for $B_4C$ (~ 1 eV/atom[10]). The interaction of secondary electrons with residual gas molecules in the XDC chamber where the exposures took place could be responsible for the apparent erosion indicated by the modeling results in Figs. 4, 5, 6. Nevertheless, the interaction of secondary electrons with residual gas molecules could also produce deposits (the opposite of erosion), such as the ones observed in the LCLS soft x-ray mirrors after prolonged exposures to the LCLS beam[13]. This once again demonstrates that the physics mechanisms and outcomes of the interaction of the LCLS beam with the mirror coatings may be highly dependent on the beam parameters, exposure times and environmental conditions in the experimental chamber.

## 4. SUMMARY AND FUTURE WORK

After the successful delivery of the x-ray optics for the SXR and CXI instruments, the development and calibration of state-of-the-art, novel x-ray optics for the entire LCLS facility has now been completed. The first exposures of $B_4C$ coatings to the LCLS beam at photon energies near the carbon K-edge produced results that could be consistent with erosion or with slight modifications of the refractive index of the top few nm of the coating. To further elucidate the physics mechanisms taking place during the interaction of the LCLS beam with the x-ray mirror coatings, additional dedicated experiments would be needed with detailed monitoring and analysis of the environmental conditions and other relevant experimental parameters. Such experiments would be extremely beneficial towards improving the performance and lifetime of about 20 x-ray mirrors and gratings currently employed at the LCLS facility.

## ACKNOWLEDGEMENTS

This work was performed under the auspices of the U.S. Department of Energy by Lawrence Livermore National Laboratory under Contract DE-AC52-07NA27344 and by the University of California Lawrence Berkeley National Laboratory under Contract No. DE-AC03-76F00098. Work was supported in part by DOE Contract DE-AC02-76SF00515. Portions of this work were performed in support of the LUSI MIE project at SLAC National Accelerator Laboratory. Portions of this work were carried out for the SXR Instrument at the LCLS. The SXR Instrument is funded by a consortium whose membership includes the LCLS, Stanford University through the Stanford Institute for Materials Energy Sciences (SIMES), Lawrence Berkeley National Laboratory, University of Hamburg through the BMBF priority program FSP 301, and the Center for Free Electron Laser Science (CFEL). Portions of this research were carried out at the LCLS facility at the SLAC National Accelerator Laboratory. LCLS is an Office of Science User Facility operated for the U.S. Department of Energy Office of Science by Stanford University. The contributions to the work on carbon K-edge exposures by Rick Iverson, James Turner, Tonee Smith, Gene Kraft, Nick Krisch, Dale Gill, Dave Shelley, Denise Larson, Dentell Reed, Leo Giannini, Georg Gassner, Michael L. Gaydosh, Brian Rutledge, Rich Atkinson, Tito Torres and Ramiro Reyna Jr. (SLAC), are gratefully acknowledged.

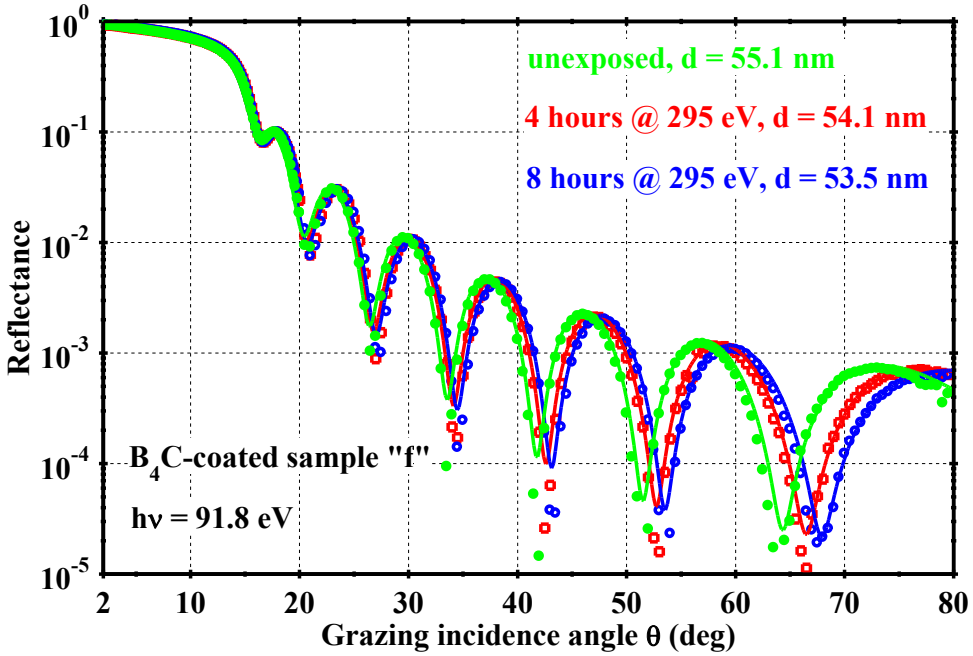


**Fig. 4:** Reflectance vs. grazing incidence angle for $B_4C$-coated sample "f". All data points are reflectance measurements at 91.8 eV obtained at ALS beamline 6.3.2. Reflectance was measured at 3 locations on the sample: (i) a location not exposed to the LCLS beam ("control" location), (ii) a location exposed to LCLS for 4 hours at 295 eV and (iii) a location exposed to LCLS for 8 hours at 295 eV. All solid lines are models[26] assuming a single layer of $B_4C$ coating[11]. The $B_4C$ coating thicknesses d (nm) shown in the legend were obtained from the models.

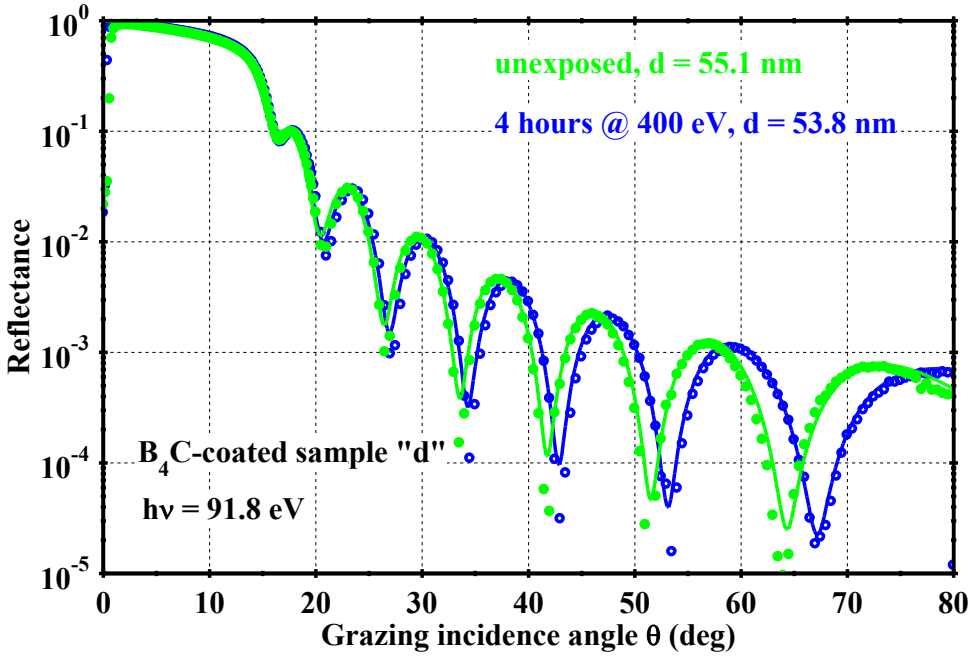


**Fig. 5:** Reflectance vs. grazing incidence angle for $B_4C$-coated sample "d". All data points are reflectance measurements at 91.8 eV obtained at ALS beamline 6.3.2. Reflectance was measured at 2 locations on the sample: (i) a location not exposed to the LCLS beam ("control" location) and (ii) a location exposed to LCLS for 4 hours at 400 eV. All solid lines are models[26] assuming a single layer of $B_4C$ coating[11]. The $B_4C$ coating thicknesses d (nm) shown in the legend were obtained from the models.

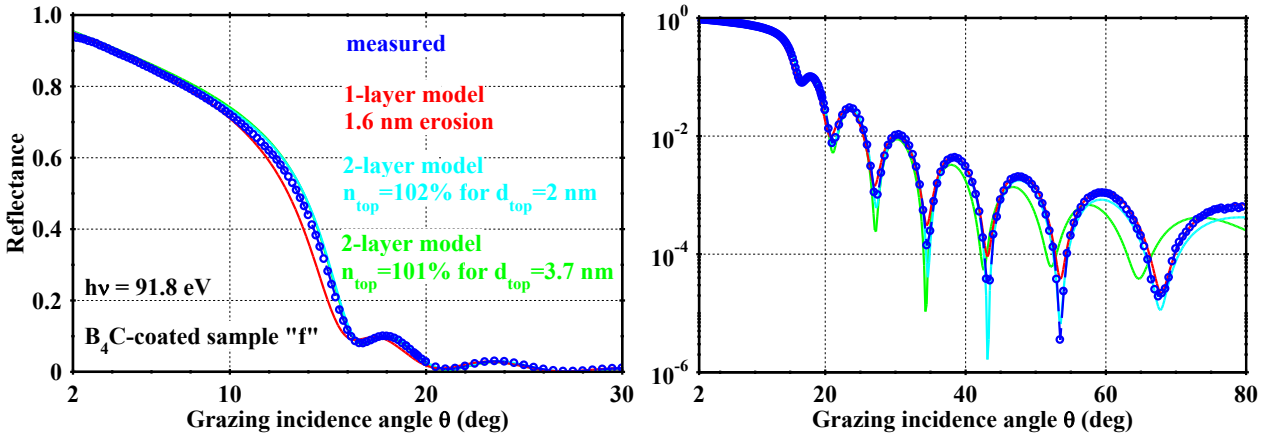


**Fig. 6:** Reflectance vs. grazing incidence angle for $B_4C$-coated sample "f". **Left:** linear reflectance axis. **Right:** logarithmic reflectance axis. The blue data points are reflectance measurements at 91.8 eV obtained at ALS beamline 6.3.2. The measurement location had earlier been exposed at LCLS for 8 hours at 295 eV. The 3 solid lines represent 3 different models of the reflectance data. (i) Red line: 1-layer model, with $B_4C$ coating thickness d = 53.5 nm. The original, unexposed $B_4C$ thickness was 55.1 nm (Fig. 4). (ii) Light blue line: 2-layer $B_4C$ coating model, with layer thicknesses $d_{top}$= 2 nm (top layer, with refractive index $n_{top}$= 102% of $B_4C$ refractive index[11]) and $d_{bottom}$= 53.1 nm (bottom layer). (iii) Green line: 2-layer $B_4C$ coating model, with layer thicknesses $d_{top}$= 3.7 nm (top layer, with refractive index $n_{top}$=101% of $B_4C$ refractive index[11]) and $d_{bottom}$= 51.4 nm (bottom layer). In models (ii) and (iii), the original $B_4C$ coating thickness d = 55.1 nm (the sum of the top and bottom layer thicknesses) is maintained after the LCLS exposure.

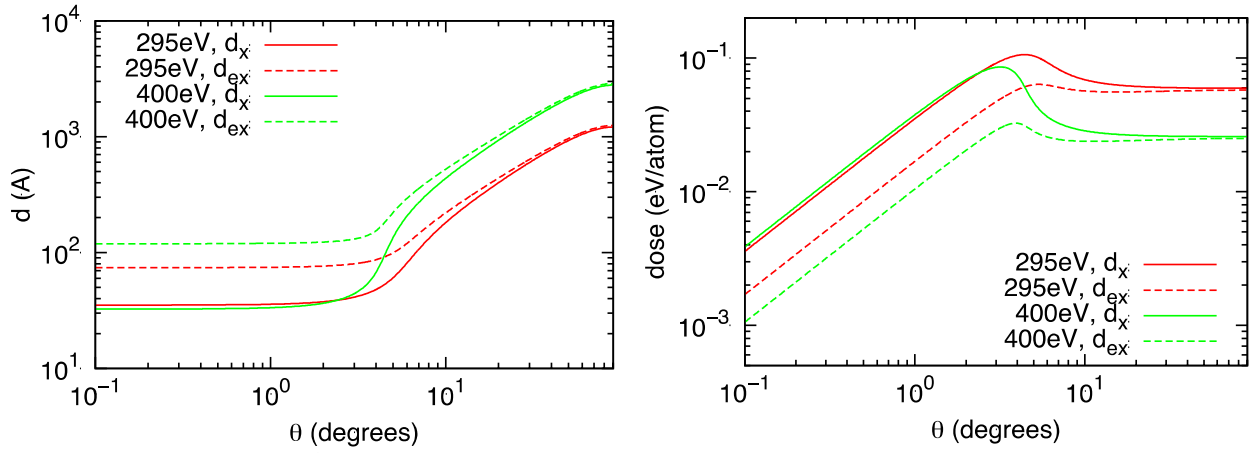


**Fig. 7: Left:** Penetration depth (Å) is plotted as a function of grazing incidence angle of the LCLS beam for two photon energies, 295 eV and 400 eV. $d_x$ is used for the penetration depth of x-rays and $d_{ex}$ is used for the combined penetration depth of electrons and x-rays. **Right:** Estimated dose (eV/atom) for the penetration depths shown on the left plot.

## REFERENCES


[1] http://lcls.slac.stanford.edu/

[2] M. Pivovaroff, R. M. Bionta, T. J. Mccarville, R. Soufli, P. M. Stefan, "Soft X-ray mirrors for the Linac Coherent Light Source", Proc. SPIE **6705**, 67050O (2007).

[3] R. Soufli, M. J. Pivovaroff, S. L. Baker, J. C. Robinson, E. M. Gullikson, T. J. McCarville, P. M. Stefan, A. L. Aquila, J. Ayers, M. A. McKernan, R. M. Bionta, "Development, characterization and experimental performance of x-ray optics for the LCLS free-electron laser" Proc. SPIE **7077,** 707716 (2008).

[4] T. J. McCarville, P. M. Stefan, B. Woods, R. M. Bionta, R. Soufli, M. J. Pivovaroff, "Opto-mechanical design considerations for the Linac Coherent Light Source X-ray mirror system", Proc. SPIE **7077** 70770E (2008).

[5] A. Barty, R. Soufli, T. McCarville, S. L. Baker, M. J. Pivovaroff, P. Stefan and R. Bionta, "Predicting the coherent X-ray wavefront focal properties at the Linac Coherence Light Source (LCLS) X-ray free electron laser", Optics Express **17**, 15508-15519 (2009).

[6] S. Hau-Riege, "Absorbed XFEL dose in the components of the LCLS X-Ray optics." LLNL report: UCRLTR-215833; http://www.llnl.gov/tid/lof/documents/pdf/325503.pdf, October 2005.

[7] S. P. Hau-Riege, R. A. London, R. M. Bionta, M. A. McKernan, S. L. Baker, J. Krzywinski, R. Sobierajski, R. Nietubyc, J. B. Pelka, M. Jurek, L. Juha, J. Chalupsky, J. Cihelka, V. Hajkova, A. Velyhan, J. Krasa, J.Kuba, K. Tiedtke, S. Toleikis, T.Tschentscher, H. Wabnitz, M. Bergh, C. Caleman, K. Sokolowski-Tinten, N. Stojanovic, and U. Zastrau, "Damage threshold of inorganic solids under free-electron-laser irradiation at 32.5 nm wavelength," App. Phys. Lett. **90**, 173128 (2007).

[8] S. P. Hau-Riege, R. A. London, R. M. Bionta, R. Soufli, D. Ryutov, M. Shirk, S. L. Baker, P. M. Smith, and P. Nataraj, "Multiple pulse thermal damage thresholds of materials for x-ray free electron laser optics investigated with an ultraviolet laser", Appl. Phys. Lett. **93**, 201105 (2008).

[9] S.P. Hau-Riege, R.A. London, R.M. Bionta, D. Ryutov, R. Soufli, S. Bajt, M.A. McKernan, S.L. Baker, J. Krzywinski, R. Sobierajski, R. Nietubyc, J. B. Pelka, M. Jurek, L. Juha, J. Chalupský, J. Cihelka, V. Hájková, A. Velyhan, J. Krása, J. Kuba, K. Tiedtke, S. Toleikis, H. Wabnitz, M. Bergh, C. Caleman, N. Timneanu,"Wavelength dependence of the damage threshold of inorganic materials under extreme-ultraviolet free-electron-laser irradiation", Appl. Phys. Lett. **95**, 111104 (2009).

[10] S. P. Hau-Riege, R.A. London, A. Graf, S. L. Baker, R. Soufli, R. Sobierajski, T. Burian, J. Chalupsky, L. Juha, J. Gaudin, J. Krzywinski, S. Moeller, M. Messerschmidt, J. Bozek, and Ch. Bostedt," Interaction of low-Z inorganic solids with short x-ray pulses at the LCLS free-electron laser", Optics Express **18**, 23933-23938 (2010).

[11] R. Soufli, A. L. Aquila, F. Salmassi, M. Fernández-Perea, E. M. Gullikson, "Optical constants of magnetron sputtered boron carbide thin films from photoabsorption data in the range 30 to 770 eV", Appl. Opt. **47**, 4633-4639 (2008).

[12] R. Soufli, S. L. Baker, J. C. Robinson, E. M. Gullikson, T. J. McCarville, M. J. Pivovaroff, P. Stefan, S. P. Hau-Riege, R. Bionta, "Morphology, microstructure, stress and damage properties of thin film coatings for the LCLS x-ray mirrors", Proc. SPIE **7361,** 73610U (2009).
[13] R. Soufli, M. Fernández-Perea, S. P. Hau-Riege, S. L. Baker, J. C. Robinson, E. M. Gullikson, J. D. Bozek, N. M. Kelez, S. Boutet, "Lifetime and damage threshold properties of reflective x-ray coatings for the LCLS free-electron laser", Proc. SPIE **8077**, 807702 (2011).
[14] R. Soufli, M. Fernández-Perea, S. L. Baker, J. C. Robinson, E. M. Gullikson, P. Heimann, V. V. Yashchuk, W. R. McKinney, W. F. Schlotter and M. Rowen, "Development and calibration of mirrors and gratings for the Soft X-Ray Materials Science beamline at the Linac Coherent Light Source free-electron laser", Appl. Opt. **51**, 2118-2128 (2012).
[15] R. Soufli, R. M. Hudyma, E. Spiller, E. M. Gullikson, M. A. Schmidt, J. C. Robinson, S. L. Baker, C. C. Walton, and J. S. Taylor "Sub-diffraction-limited multilayer coatings for the 0.3 numerical aperture micro-exposure tool for extreme ultraviolet lithography", Appl. Opt. **46**, 3736-3746 (2007).
[16] W. F. Schlotter, J. J. Turner, M. Rowen, P. Heimann, M. Holmes, O. Krupin, M. Messerschmidt, S. Moeller, J. Krzywinski, R. Soufli, M. Fernández-Perea, N. Kelez, S. Lee, R. Coffee, G. Hays, M. Beye, N. Gerken, F. Sorgenfrei, S. Hau-Riege, L. Juha, J. Chalupsky, V. Hajkova, A. P. Mancuso, A. Singer, O. Yefanov, I. A. Vartanyants, G. Cadenazzi, B. Abbey, K. A. Nugent, H. Sinn, J. Lüning, S. Schaffert, S. Eisebitt, W.-S. Lee, A. Scherz, A. R. Nilsson, and W. Wurth "The soft x-ray instrument for materials studies at the linac coherent light source x-ray free-electron laser", Rev. Sci. Instrum. **83**, 043107 (2012).
[17] P. Heimann, O. Krupin, W. F. Schlotter, J. Turner, J. Krzywinski, F. Sorgenfrei, M. Messerschmidt, D. Bernstein, J. Chalupský, V. Hájková, S. Hau-Riege, M. Holmes, L. Juha, N. Kelez, J. Lüning, D. Nordlund, M. Fernandez Perea, A. Scherz, R. Soufli, W. Wurth, and M. Rowen "Linac Coherent Light Source soft x-ray materials science instrument optical design and monochromator commissioning", Rev. Sci. Instrum. **82**, 093104 (2011).
[18] J. L. Kirschman, E. E. Domning, W. R. McKinney, G. Y. Morrison, B. V. Smith, and V. V. Yashchuk, "Performance of the upgraded LTP-II at the ALS Optical Metrology Laboratory," Proc. SPIE **7077**, 70770A (2008).
[19] S. Boutet and G. Williams "The Coherent X-ray Imaging (CXI) instrument at the Linac Coherent Light Source (LCLS)", New Journal of Physics **12**, 035024 (2010).
[20] K. Yamauchi, H. Mimura, K. Inagaki, and Y. Mori, "Figuring with subnanometer-level accuracy by numerically controlled elastic emission machining", Rev. Sci. Instrum. **73**, 4028 (2002).
[21] D. L. Windt, "topo - surface topography analysis", available at http://www.rxollc.com/idl/index.html
[22] F. Siewert, J. Buchheim, S. Boutet, G. J. Williams, P. A. Montanez, J. Krzywinski, and R. Signorato, "Ultra-precise characterization of LCLS hard X-ray focusing mirrors by high resolution slope measuring deflectometry", Opt. Exp. **20**, 4525-4536 (2012).
[23] I. Horcas, R. Fernández, J.M. Gómez-Rodríguez, J. Colchero, J. Gómez-Herrero, and A.M. Baro, "WSXM: A software for scanning probe microscopy and a tool for nanotechnology", Rev. Sci. Instrum **78**, 013705 (2007).
[24] A. F. G. Leontowich and A. P. Hitchcock, "Secondary electron deposition mechanism of carbon contamination", J. Vac. Sci. Technol. B **30**(3), 030601 (2012).
[25] E. M. Gullikson, S. Mrowka, B. B. Kaufmann, "Recent developments in EUV reflectometry at the Advanced Light Source," Proc. SPIE **4343**, 363-373 (2001).
[26] D. L. Windt, "IMD: Software for modeling the optical properties of multilayer films," Computers in Physics **12**, 360–370, 1998. Available at http://www.rxollc.com/idl/index.html.
[27] S. P. Hau-Riege, "High-Intensity X-rays – Interaction with Matter", Wiley-VCH (2011).
[28] E. J. Kobetich and R. Katz, "Energy Deposition by Electron Beams and δ Rays", Phys. Rev. B **170**, 391-396 (1968).